

Article

Single-Atom X/g-C₃N₄ (X = Au₁, Pd₁, and Ru₁) Catalysts for Acetylene Hydrochlorination: A Density Functional Theory Study

Xuening Zhou^{1,2}, Mingyuan Zhu¹ and Lihua Kang^{1,*}

¹ School of Chemistry and Chemical Engineering of Shihezi University, Shihezi 832000, China; zhouxuening@stu.shzu.edu.cn (X.Z.); zhumin Yuan@shzu.edu.cn (M.Z.)

² Key Laboratory for Green Processing of Chemical Engineering of Xinjiang Bingtuan, Shihezi 832000, China

* Correspondence: kanglihua@shzu.edu.cn; Tel.: +86-099-3205-7213; Fax: +86-099-3205-7270

Received: 12 September 2019; Accepted: 25 September 2019; Published: 26 September 2019



Abstract: The mechanisms of the single-atom X/g-C₃N₄ (X = Au₁, Pd₁, and Ru₁) catalysts for the acetylene hydrochlorination reaction were systematically investigated using the density functional theory (DFT) B3LYP method. The density functional dispersion correction obtained by the DFT-D3 method was taken into account. During the reaction, C₂H₂ and HCl were well activated and the analysis of the adsorption energy demonstrated the adsorption performance of C₂H₂ is better than that of HCl. The catalytic mechanisms of the three catalysts consist of one intermediate and two transition states. Moreover, our results showed that the three single-atom catalysts improve the catalytic activity of the reaction to different degrees. The calculated energy barrier declines in the order of Pd₁/g-C₃N₄ > Ru₁/g-C₃N₄ > Au₁/g-C₃N₄, and the energy barrier for the Au₁/g-C₃N₄ catalyst was only 13.66 kcal/mol, proving that single-atom Au₁/g-C₃N₄ may be a potential catalyst for hydrochlorination of acetylene to vinyl chloride.

Keywords: single-atom; X/g-C₃N₄ (X = Au₁; Pd₁; and Ru₁) catalysts; acetylene hydrochlorination; DFT-D3; catalytic activity

1. Introduction

With the rapid development of industrial catalysis, it is imperative to find a cost-effective catalyst for catalytic reactions. Single-atom catalysts (SACs) stand out due to their low cost, high activity, high selectivity, and clear active centers [1]. Another advantage of SACs is the 100% utilization, as they consist of a single isolated metal atom supported on the carrier. They greatly improve the efficiency of the metal atoms and offer a number of advantages over the conventional supported noble metal catalysts [2,3]. Huang et al. [4] synthesized a single-atom silver chain with high catalytic ability by simple thermal treatment of silver, which also resulted in excellent formaldehyde oxidation activity at low temperature. Qiao et al. [5] dispersed a single Pt atom on large surface area FeO_x carrier to form Pt₁/FeO_x catalyst, which displayed high activity for both preferential oxidation reactions and CO oxidation. Yang et al. [6] deposited an isolated gold atom on a titania carrier and suspended it in ethanol for a low-temperature catalytic water–gas conversion. Gao et al. [7] reported that single-atom Pd supported on graphite carbon nitride is an effective photocatalyst for visible light reduction of CO₂. SACs exhibit good performance in many heterogeneous reactions; therefore, they have potential to be applied in a wide range of processes. Until now, little research has been done on the acetylene hydrochlorination using SACs, and particularly on the theoretical mechanism of this reaction [8–13].

Polyvinyl chloride (PVC) plays an important role in various applications. Its vinyl chloride monomer (VCM) is mainly synthesized by the calcium carbide method, with mercury chloride as

the catalyst [9,14]. However, due to the toxicity of mercury chloride, as well as its sublimation at high temperatures, its use is hazardous to human health and the environment [15]. Therefore, the application of non-mercury-based catalyst in the synthesis of VCM is imperative [16]. In the late 20th century, Hutchings et al. [17] proposed that gold-based catalysts may be a more environmentally friendly alternative for the hydrochlorination of acetylene. Subsequently, their experiments [18] showed that AuCl_3 was the optimal catalyst for this reaction. In 2013, Kang et al. [19] studied the reaction mechanism of acetylene hydrochlorination on MCl_x ($\text{M} = \text{Hg}, \text{Au}, \text{Ru}; x = 2, 3$) catalyst and validated this conclusion. Moreover, the group also proposed that an Ru-based catalyst may be another promising candidate [20]. Theoretical and experimental studies on the hydrochlorination of acetylene using Ru-based catalysts have also been carried out previously [21–26]. Furthermore, Pd-based catalysts have been extensively studied in the past. In 2013, Wang et al. [27] synthesized a palladium catalyst supported on Y zeolite for the preparation of vinyl chloride, which displayed high conversions and selectivity. Following this, NH_4F was added to modify the catalyst, improving its catalytic performance [28]. Moreover, in 2015, Hu et al. [29] reported that confining metal Pd nanoparticles (Pd NPs) in surfactant ionic liquids resulted in excellent catalytic performance in the acetylene hydrochlorination reaction. The good performance of the Au, Pd, and Ru metals suggests that they can be suitable for SACs applications.

In addition, Wang et al. [30] indicated that among Au_{3-10} clusters, the Au_3 cluster was the best catalyst for chlorination of acetylene. Zhao et al. [31] studied the effects of Si atom doping into Au_7 (Au_6Si) and Au_8 (Au_7Si) clusters on their catalytic activities in the acetylene hydrochlorination reaction. Their investigation revealed that, as well as altering the size and shape of metal atoms, doping is also an excellent approach for modifying catalysts. Furthermore, Zhao et al. [32] showed that Au_3/N -graphene exhibited good performance in catalyzing the acetylene hydrochlorination reaction. In addition, Gong et al. [8] reported that N-doped AuG-SACs displayed great potential as catalysts in the synthesis of vinyl chloride, which was, therefore, considered as a candidate catalyst. This outcome further confirms our hypothesis that further research into utilizing SACs for catalyzing hydrochlorination of acetylene is necessary.

Graphitic carbon nitride ($\text{g-C}_3\text{N}_4$) is considered as an excellent catalyst carrier due to its good thermochemical stability, large surface area, abundant reserves, low cost, and easy capture of single active metal [33–35]. Li et al. [36] used activated carbon (AC) to support the $\text{g-C}_3\text{N}_4$ catalyst for the acetylene hydrochlorination reaction, and obtained higher catalytic activity than using AC alone. Subsequently, Zhao et al. [37] described the addition of CuCl_2 to $\text{g-C}_3\text{N}_4/\text{AC}$ for the preparation of vinyl chloride. Their results showed that the resulting $\text{Cu-g-C}_3\text{N}_4/\text{AC}$ catalyst displayed better catalytic performance than the aforementioned $\text{g-C}_3\text{N}_4/\text{AC}$ catalyst. Moreover, the properties of the $\text{M/g-C}_3\text{N}_4$ single-atom catalyst formed by embedding transition metal into monolayer $\text{g-C}_3\text{N}_4$ were also examined [38,39]. All of the described studies encouraged us to embed the Au, Pd, and Ru metals in $\text{g-C}_3\text{N}_4$ to form SACs for acetylene hydrochlorination reaction. In the present work, we use a density functional theory (DFT) method to evaluate the adsorption characteristics of C_2H_2 and HCl on single-atom $\text{X/g-C}_3\text{N}_4$ ($\text{X} = \text{Au}_1, \text{Pd}_1, \text{and Ru}_1$) catalysts, as well as to study the reaction pathway and the mechanism of acetylene hydrochlorination. Furthermore, we compare the catalytic activity of each of the three catalysts. Our work gives a deeper understanding of monoatomic catalysts and provides some inspiration for the future design of monoatomic catalysts for acetylene hydrochlorination.

2. Computational Methods

In the current work, all simulations of density functional theory (DFT) were performed by using the Gaussian09 software package [40]. The processes involved geometrical optimization without symmetry constraints. The geometrical optimization of the system studied in this work was carried out for all the atoms at the same time, using the B3LYP density functional theory, which is described by Lee, Yang, and Parr [41] to obtain the electron density while electronic states for each type of atom are described by different types of basis sets (6-31G** for non-metals; the effective core pseudo-potential

of Los Alamos LANL2DZ for metals). To improve the accuracy of the results, the density functional dispersion correction using the DFT-D3 method was taken into account [42]. All relative energies of the optimized structures in the whole reaction path are zero-point energy corrections at the B3LYP/6-31G** level and also with the DFT-D3 method. Using the Hessian calculation at the same level, the stationary points were characterized as minima (no virtual frequency) or transition states (only one virtual frequency). Intrinsic reaction coordinate (IRC) [43,44] calculations were used to ensure that each transition state linked the corresponding products with the reactants in the process of calculation.

An essential reference point for this calculation was the adsorption energy for HCl and C₂H₂ adsorbed on single-atom X/g-C₃N₄ (X = Au₁, Pd₁, and Ru₁) catalysts. In this study, we define adsorption energy (*E*_{ads}) and co-adsorption energy (*E*_{co-ads}) as follows:

$$E_{ads} = E_{ads\ state} - (E_{C_2H_2/HCl} + E_{catalyst}) \quad (1)$$

$$E_{co-ads} = E_{co-ads\ state} - (E_{C_2H_2} + E_{HCl} + E_{catalyst}) \quad (2)$$

where *E*_{ads state} and *E*_{co-ads state} are the total energy values of the reactant and catalyst systems, whereas *E*_{catalyst}, *E*_{C₂H₂} and *E*_{HCl} are the energy values of the isolated catalyst and reactants.

3. Results and Discussion

3.1. Geometrical Structure of the Reactants

The reactants, including the isolated C₂H₂ molecule, HCl molecule, and single-atom X/g-C₃N₄ (X = Au₁, Pd₁, and Ru₁) catalysts, as well as the optimized structures are shown in Figure 1. As previously reported, triazine and tri-s-triazine are two basic structural units of g-C₃N₄ [45]. To get the most stable and optimal structure of g-C₃N₄ for the simulation study, we initially chose three adjacent tri-s-triazine layered units. Similarly, to the structure employed previously by our group [46], we also used a wave-like structure in the current work [47]. In addition, in the structures we calculated, all the structures containing metal Au are doublet states, and the other structures such as C₂H₂ molecule, HCl molecule, g-C₃N₄ molecule and the structures containing metal Pd and Ru are all singlet states.

By placing the three investigated metals in all possible locations of the labeled atoms in g-C₃N₄ Figure 1a, the three lowest energy structures of the catalysts were obtained. As shown in Figure 1b–d, Au, Pd, and Ru all tend to adsorb in a six-fold cavity of g-C₃N₄, which is consistent with a previous report [39]. The Au atom is located roughly in the middle of g-C₃N₄ and is not connected to any other atom (Figure 1b). Furthermore, the Au-C1 distance is 3.34 Å, both Au-N1 and Au-N6 distance are 3.42 Å, Au-N2 and Au-N5 are 3.10 Å, and Au-N3 and Au-N4 are 3.29 Å. The Pd atom is bonded to C1 by the chemical bond of 1.5 Å (Figure 1c). The bond lengths of Pd-N1 and Pd-N6, Pd-N2 and Pd-N5, and Pd-N3 and Pd-N4 are similar, specifically 2.51 Å, 2.54 Å, and 3.01 Å, respectively. The Ru atom is connected to N3 and N4 by 1.94 Å bonds (Figure 1d). Ru-C1 has a distance of 3.51 Å, similarly Ru-N1 and Ru-N6, and Ru-N2 and Ru-N5 have the same bond lengths of 3.19 Å and 2.64 Å. Moreover, the structures of the three catalysts obtained by adding Au, Pd and Ru are different from the original g-C₃N₄, and all of them display varying degrees of deformation. Our results; therefore, indicate the presence of a strong interaction between the metal and the carrier.

As can be seen from the highest occupied molecular orbital (HOMO) shown in Figure 2, the charge distribution in g-C₃N₄ is relatively uniform. It is clear, however, that following their introduction, the charge is concentrated mainly on the metal atoms. This indicates an obvious charge transfer between the metal atoms and the g-C₃N₄ carrier. Figure 2 shows the “s” character of HOMO at Au and Ru, and “d” character at Pd. This correlates with electron configuration of atoms 5d¹⁰s¹, 4d¹⁰s⁰, and 4d⁷s¹ for Au, Pd, and Ru, respectively. The larger diameter of the sphere of the HOMO on Au than on Ru correlates with higher electronegativity of Au (2.54 versus 2.20). The large diameter and spherical shape of the HOMO leads to the central position of the Au atom in the hole. Bonding of Au is therefore

more ionic in contrast to Pd and Ru, where bonding is more covalent. Another feature visible in Figure 2 is that covalent bonding of Pd is of sigma character and bonding of Ru is of pi character.

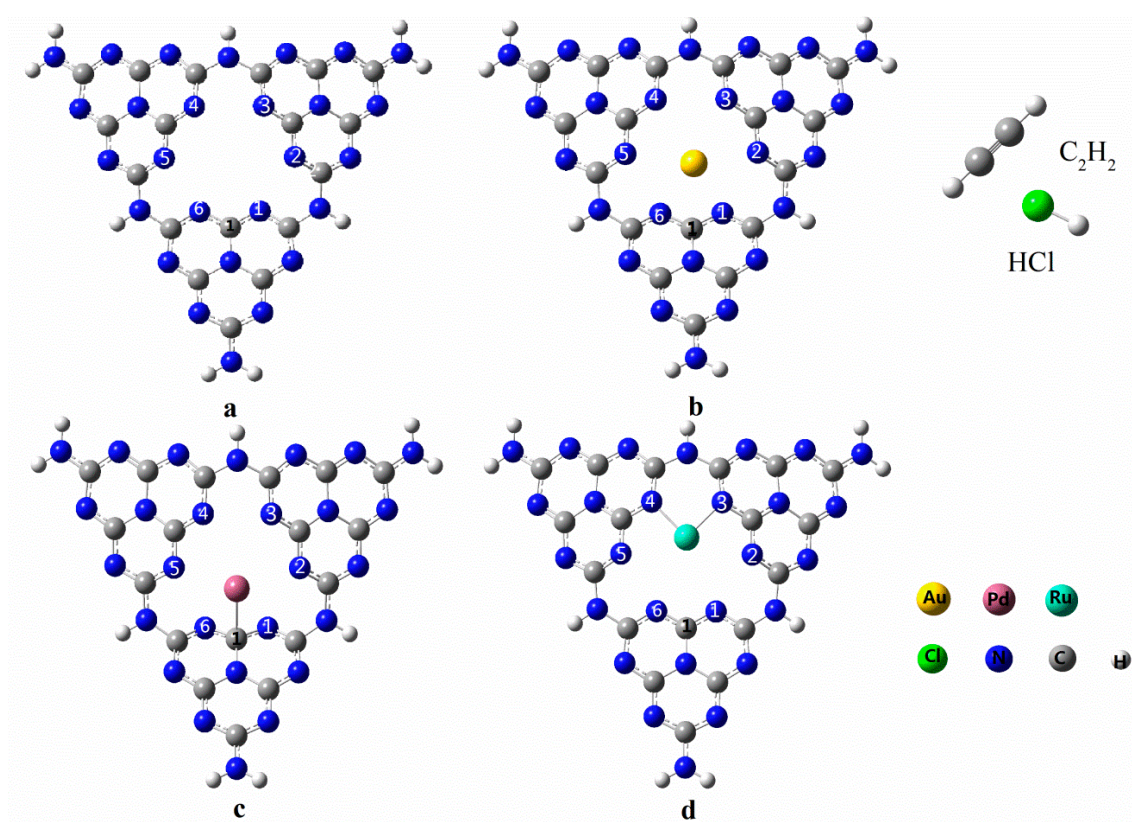


Figure 1. The optimized structures of acetylene (C_2H_2), hydrogen chloride (HCl), graphite carbon nitride ($g-C_3N_4$) (a), $Au_1/g-C_3N_4$ (b), $Pd_1/g-C_3N_4$ (c), and $Ru_1/g-C_3N_4$ (d).

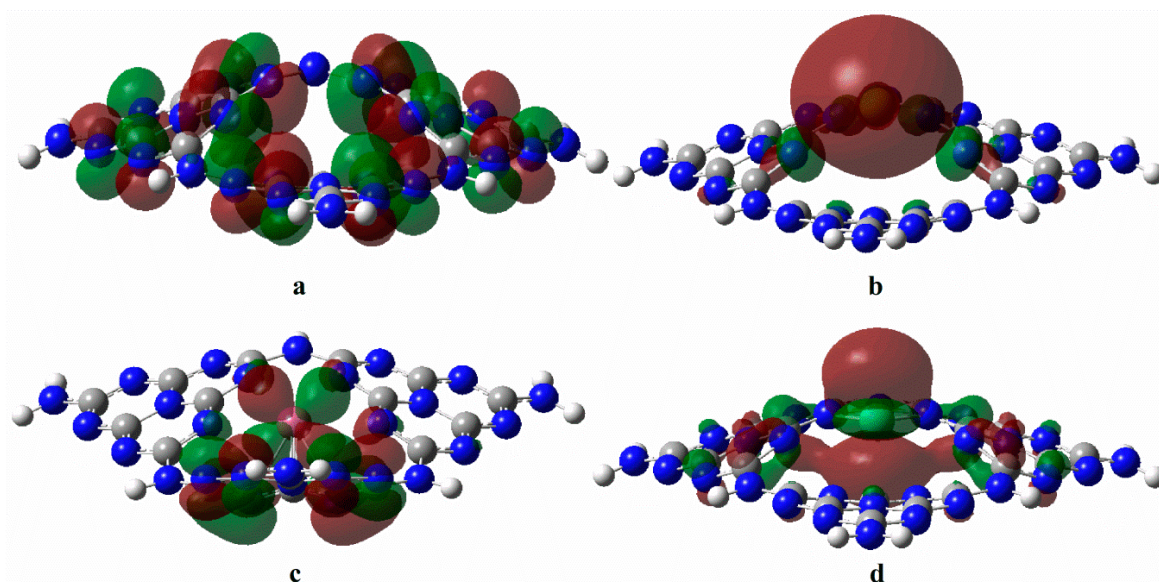


Figure 2. Frontier molecular orbitals of HOMO for $g-C_3N_4$ (a), $Au_1/g-C_3N_4$ (b), $Pd_1/g-C_3N_4$ (c), and $Ru_1/g-C_3N_4$ (d).

3.2. Adsorption of C_2H_2 and HCl onto SACs

To clarify the adsorption strength of C_2H_2 and HCl, we examined the individual optimal adsorption energy values for C_2H_2 and HCl (Table 1). The results demonstrate that the adsorption energies of

C_2H_2 are higher than those of HCl, indicating that the adsorption performance of C_2H_2 is better than that of HCl. Adsorption energy of C_2H_2 correlates with the number of empty d-orbitals which are available for bonding. Furthermore, with a view to obtaining the optimal adsorption site structures of C_2H_2 and HCl, we placed them in different positions on the SACs. The resulting structures are presented in Figure 3. It can be seen that both C_2H_2 and HCl are adsorbed on the metal atoms of SACs, suggesting that the metal atoms are the only active sites on the catalysts. This finding is in agreement with the previous research [38]. As a consequence of the adsorption of C_2H_2 , all of the $C\equiv C$ triple bonds turned into double bonds, hence the bond lengths changed from 1.21 Å to 1.24 Å, 1.26 Å and 1.32 Å for $Au_1/g-C_3N_4\cdot C_2H_2$, $Pd_1/g-C_3N_4\cdot C_2H_2$, and $Ru_1/g-C_3N_4\cdot C_2H_2$, respectively. As for HCl, the bond lengths increased from 1.29 Å to 1.38 Å, 1.52 Å, 1.30 Å for $Au_1/g-C_3N_4\cdot HCl$, $Pd_1/g-C_3N_4\cdot HCl$, and $Ru_1/g-C_3N_4\cdot HCl$, respectively. All these changes demonstrate that single atoms deposited on the support are strong active sites.

Table 1. The optimal adsorption energies of C_2H_2 and HCl adsorbed separately and co-adsorbed on the single-atom catalysts (SACs) (energies in kcal/mol).

	C_2H_2	HCl	Co-Adsorption
$Au_1/g-C_3N_4$	-14.07	-10.64	-26.38
$Pd_1/g-C_3N_4$	-28.08	-12.70	-43.32
$Ru_1/g-C_3N_4$	-35.81	-3.38	-51.38

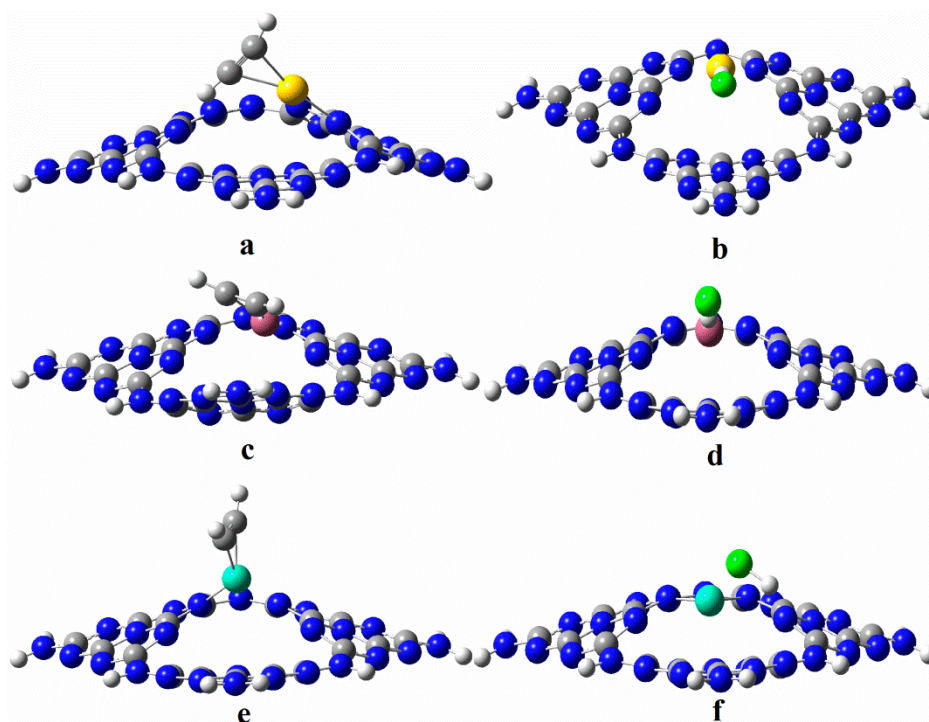


Figure 3. The stable adsorption configurations of $Au_1/g-C_3N_4\cdot C_2H_2$ (a), $Au_1/g-C_3N_4\cdot HCl$ (b), $Pd_1/g-C_3N_4\cdot C_2H_2$ (c), $Pd_1/g-C_3N_4\cdot HCl$ (d), $Ru_1/g-C_3N_4\cdot C_2H_2$ (e), and $Ru_1/g-C_3N_4\cdot HCl$ (f).

3.3. The Possible Reaction Mechanisms for Acetylene Hydrogenation on SACs

The possible reaction pathways are systematically explored and analyzed to gain a better understanding of the reaction mechanisms for acetylene hydrochlorination using $Au_1/g-C_3N_4$, $Pd_1/g-C_3N_4$, and $Ru_1/g-C_3N_4$ catalysts. Figure 4 depicts the reaction energy pathways starting from C_2H_2 and HCl co-adsorption structures. Additionally, the structures of the various stationary points located on the potential energy surface are displayed in Figures 5–7, respectively.

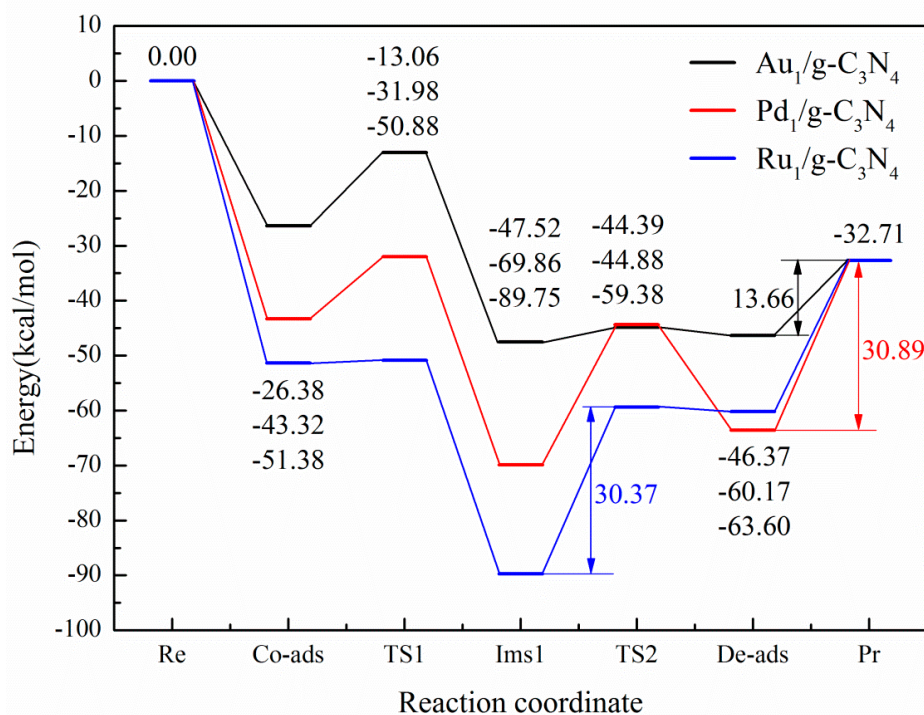


Figure 4. The energy diagrams of the most favorable pathways of acetylene hydrochlorination on Au₁/g-C₃N₄, Pd₁/g-C₃N₄, and Ru₁/g-C₃N₄: Reactants (Re), co-adsorbed reactants (co-ads), transition states (TS), intermediate (Ims), desorption products (De-ads), and products (Pr). The data are zero-point-energy (ZPE) in kcal/mol.

3.3.1. Reaction Mechanism Utilizing Au₁/g-C₃N₄

As the adsorption of C₂H₂ was shown to be better than that of HCl, C₂H₂ adsorbed on Au₁/g-C₃N₄ to form Au₁/g-C₃N₄-C₂H₂ first, followed by adsorption of HCl on Au₁/g-C₃N₄-C₂H₂ to form a co-adsorption state (Co-ads). The co-adsorption energy $E_{\text{Co-ads}}$ is -26.38 kcal/mol. As it can be seen in Figure 5, the C₂H₂ molecule has undergone an obvious topographic change, in the co-adsorption structure, indicating strong adsorption of this compound. The adsorbed HCl is located roughly in the middle of the C1-C2 bond and is nearly perpendicular to it. Considering the change in the C3-Cl bond length was less than 0.1 Å, the HCl molecule was not activated. The co-adsorption structure can be transformed into intermediate state 1 (Ims1) through a transition state 1 (TS1). The H3-Cl bond breaks in the TS1 state, and the bond length increases from 1.31 Å to 1.58 Å. Meanwhile, the H3 atom is in close proximity to the C1 atom, and the distance of H3-C1 decreases from 2.19 Å to 1.37 Å, proving that the HCl molecule is completely dissociated and activated.

Through vibrational analysis of the TS1 structure, we acquired only one imaginary frequency (-873.76 cm^{-1}). This frequency is related to the stretching vibration of the H3 atom. To reach the TS1 state, a 13.32 kcal/mol energy barrier must be overcome. The IRC calculation was executed to ensure that the TS1 links the correct co-adsorption structure and Ims1. During the transition from TS1 to Ims1, the H3 atom gradually approaches C1 and bonds to it, forming C₂H₃. Interestingly, with the formation of the H3-C1 bond, C₂H₃ reverses anticlockwise, resulting in connection of the C2 atom with Au, instead of C1. As shown in Figure 5, the HCl molecule in the Ims1 separates into two atoms, and the distance between the two atoms increases from 1.58 Å to 2.42 Å, compared to TS1.

The 2.64 kcal/mol energy barrier must be then overcome to transition from Ims1 to TS2. Following this, the distance between the C2 and Cl atoms decreases from 2.83 Å to 2.25 Å. Through the vibrational analysis of TS2, only one virtual frequency (-165.85 cm^{-1}) was obtained, which is connected with the vibration stretching from Cl to C2. The result of the IRC calculation demonstrated that TS2 can link the Ims1 and the desorption state (De-ads). The C₂H₃Cl product in the desorption state adsorbed

onto $\text{Au}_1/\text{g-C}_3\text{N}_4$ to form adsorption complexes. The C2–Cl bond length of the $\text{C}_2\text{H}_3\text{Cl}$ molecule was determined at 1.88 Å, which is longer than the same bond in the isolated $\text{C}_2\text{H}_3\text{Cl}$ molecule (1.75 Å). The ultimate step involves desorption of the $\text{C}_2\text{H}_3\text{Cl}$ molecule. The desorption energy was determined at 13.66 kcal/mol, which is the rate-limiting step. In addition, the desorption energy is equal to the adsorption energy of the $\text{C}_2\text{H}_3\text{Cl}$ molecule adsorbed onto $\text{Au}_1/\text{g-C}_3\text{N}_4$. As the adsorption energy of $\text{C}_2\text{H}_3\text{Cl}$ is low, it is easy for the products to desorb from the catalysts.

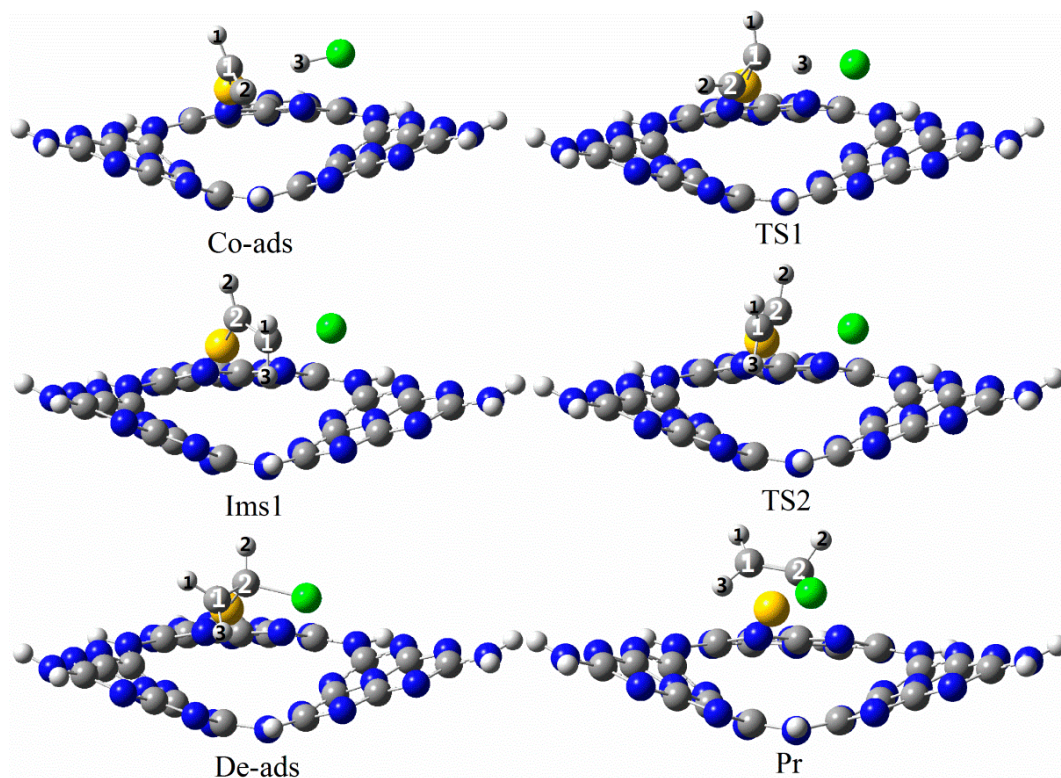


Figure 5. The energy diagram of the optimal pathway over the $\text{Au}_1/\text{g-C}_3\text{N}_4$.

3.3.2. Reaction Mechanism Utilizing $\text{Pd}_1/\text{g-C}_3\text{N}_4$

The reaction mechanism using $\text{Pd}_1/\text{g-C}_3\text{N}_4$ is similar to that employing $\text{Au}_1/\text{g-C}_3\text{N}_4$. As shown in Figure 6, C_2H_2 is first adsorbed on $\text{Pd}_1/\text{g-C}_3\text{N}_4$, followed by adsorption of HCl to form Co-ads. The $E_{\text{Co-ads}}$ is -43.32 kcal/mol, which is much higher than the $E_{\text{Co-ads}}$ of $\text{Au}_1/\text{g-C}_3\text{N}_4$. Similarly, C_2H_2 is strongly adsorbed on the catalyst. The adsorbed HCl is also located roughly in the middle of the C1–C2 bond, nearly perpendicular to it, and is inactivated in the Co-ads state. The Co-ads structure can convert to Ims1 through TS1. The H3–Cl bond in TS1 breaks and the bond length increases from 1.38 Å to 1.71 Å. Moreover, the H3 atom approaches the C2 atom and the distance decreases from 3.02 Å to 1.38 Å. Hence, all of these observations demonstrate that the HCl molecule is fully separated and activated.

Through the vibration analysis of TS1 structure, only one virtual frequency (-739.59 cm^{-1}) value was obtained, which is associated with the H3 atom vibrating to the C2 atom. A minimum of 11.34 kcal/mol energy is required to get to the TS1 state. The IRC calculation result clearly shows that TS1 connects the Co-ads structure and Ims1 correctly. As it can be seen in Figure 6, the bond for H3–C2 is formed in Ims1. An obvious change is observed in this state, which involves the HCl molecule splitting into two isolated atoms, and the distance between them increases from 1.71 Å to 2.90 Å.

Subsequently, the 25.47 kcal/mol energy barrier must be overcome to transition from Ims1 to TS2. During the transformation, the Cl atom is close to the C1 and C2 atoms and the H2 and H3 atoms flip up anticlockwise to form TS2. The distance between C1 and Cl in TS2 decreases from 3.11 Å to 2.20 Å.

Å. Meanwhile, we obtained only one virtual frequency (-285.74 cm^{-1}) by vibrational analysis of TS2 structure, which involves the stretching movement of the Cl atom. The IRC calculation is performed once again to verify that TS2 links the Ims1 and De-ads states. The $\text{C}_2\text{H}_3\text{Cl}$ product is formed in the De-ads state, and the C1–Cl bond length is 1.81 Å , which is longer than the length of the same bond in an isolated $\text{C}_2\text{H}_3\text{Cl}$ molecule. The last step involves desorption of the $\text{C}_2\text{H}_3\text{Cl}$ molecule with desorption energy of 30.89 kcal/mol , which is equal to the adsorption energy of the $\text{C}_2\text{H}_3\text{Cl}$ molecule adsorbed onto $\text{Pd}_1/\text{g-C}_3\text{N}_4$. Same as the $\text{Au}_1/\text{g-C}_3\text{N}_4$ catalyzed process, the rate-limiting step for $\text{Pd}_1/\text{g-C}_3\text{N}_4$ is desorption of the $\text{C}_2\text{H}_3\text{Cl}$ molecule from the catalyst.

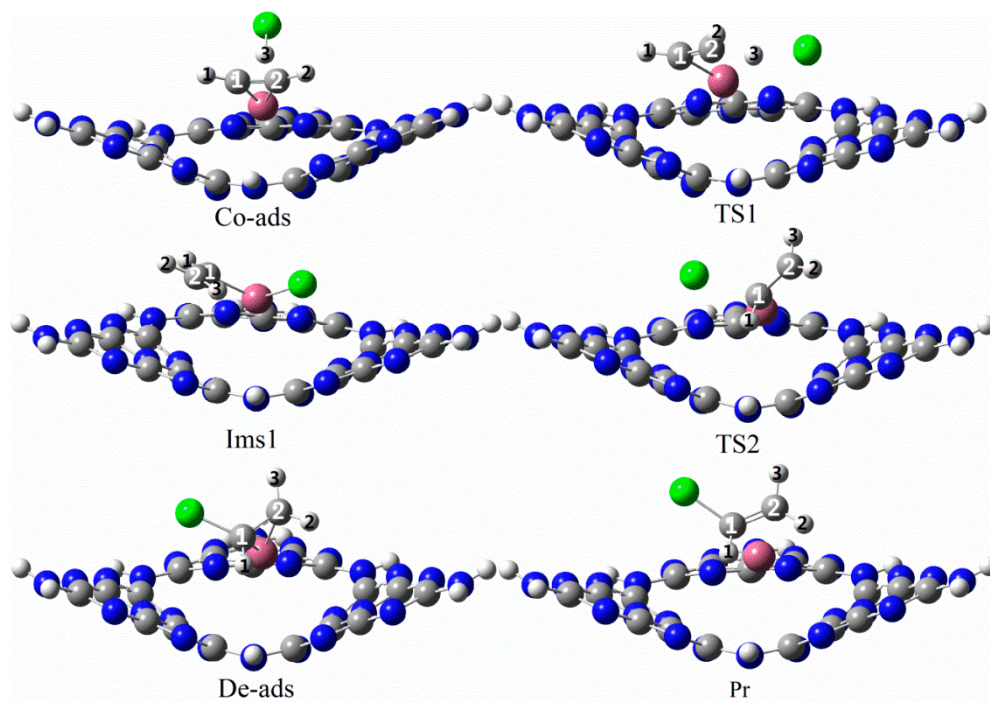


Figure 6. The energy diagram of the optimal pathway over the $\text{Pd}_1/\text{g-C}_3\text{N}_4$.

3.3.3. Reaction Mechanism Utilizing $\text{Ru}_1/\text{g-C}_3\text{N}_4$

The reaction mechanism for $\text{Ru}_1/\text{g-C}_3\text{N}_4$ is identical to the mechanisms explained above, i.e., C_2H_2 is adsorbed first, followed by the adsorption of HCl. The co-adsorption structure formed is shown in Figure 7. Unlike the previous co-adsorptions described for $\text{Au}_1/\text{g-C}_3\text{N}_4$ and $\text{Pd}_1/\text{g-C}_3\text{N}_4$, C_2H_2 and HCl are coplanar, rather than perpendicular. The $E_{\text{Co-ads}}$ is -51.38 kcal/mol , which is the largest among the three catalysts. Moreover, the C_2H_2 molecule is strongly adsorbed on $\text{Ru}_1/\text{g-C}_3\text{N}_4$ and the adsorbed HCl molecule of the Co-ads state is not activated. The Co-ads structure could transform into Ims1 through TS1. The H3–Cl bond length in TS1 increases from 1.40 Å to 1.50 Å and the C2–H3 distance decreases from 2.13 Å to 1.60 Å . These outcomes indicate that the HCl molecule is isolated and activated.

Furthermore, based on the TS1 vibration analysis, only one imaginary frequency (-527.56 cm^{-1}) was obtained, which shows the vibration of H3 to C2 in TS1. Only 0.50 kcal/mol energy is required to reach TS1. The calculation of the IRC proves that TS1 correctly connects the Co-ads and Ims1. Furthermore, HCl molecule in TS1 splits into two independent atoms, of which the H atom is bonded to C2. The distance between the two resulting atoms increases from 1.50 Å to 2.99 Å in comparison to the same distance in TS1.

To transform from Ims1 to TS2, the energy barrier of 30.37 kcal/mol must be overcome, which is the rate-limiting step of the reaction. The distance of C1–Cl in TS2 is reduced from 3.34 Å to 2.13 Å . In addition, only one imaginary frequency (-216.85 cm^{-1}) is obtained in this state based on the

vibrational analysis, which is related to the stretching movement of the Cl atom. The IRC calculation is carried out again to ensure that the TS2 links Ims1 and De-ads. The C1–Cl bond length of the C_2H_3Cl product in De-ads is 1.85 Å, which is longer than the isolated C_2H_3Cl molecule. The ultimate step involves desorption of the C_2H_3Cl product from $Ru_1/g-C_3N_4$ at 27.46 kcal/mol, which is equal to the adsorption energy of the C_2H_3Cl molecule adsorbed onto $Ru_1/g-C_3N_4$.

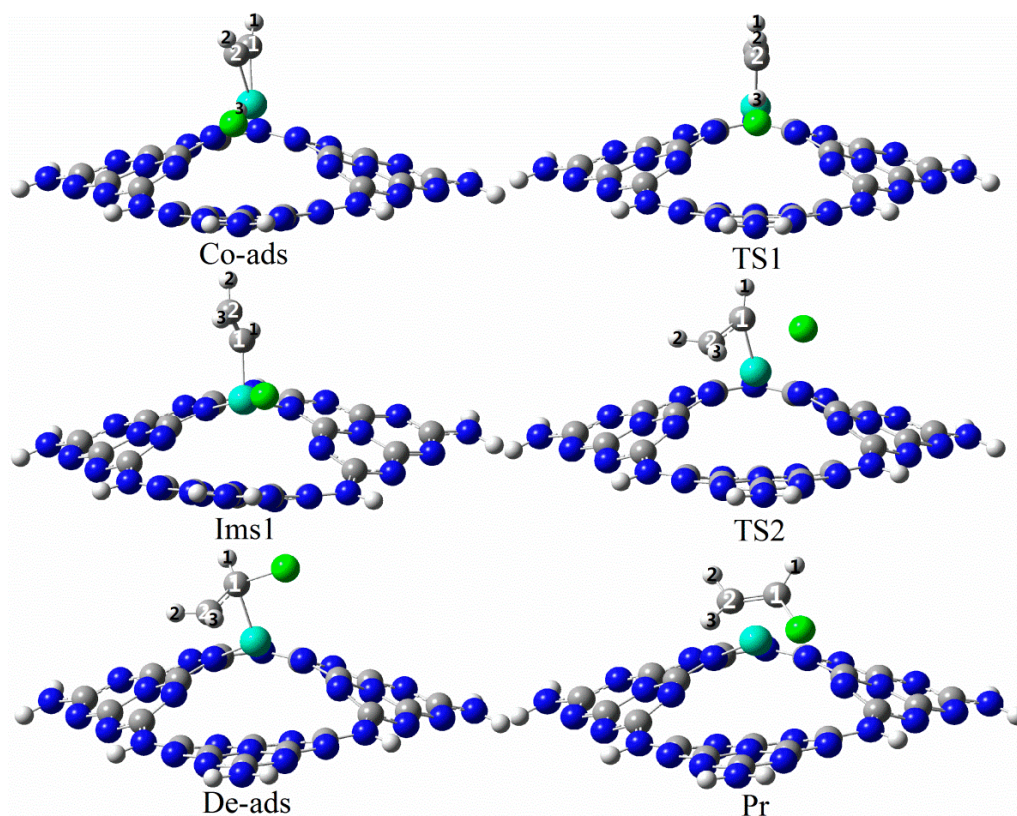


Figure 7. The energy diagram of the optimal pathway over the $Ru_1/g-C_3N_4$.

Moreover, to evaluate the catalytic activity of single-atom $X/g-C_3N_4$ ($X = Au_1, Pd_1,$ and Ru_1) in hydrochlorination of acetylene, we compared the calculated energy barriers with those of other catalysts, as shown in Table 2. Our results demonstrate that single-atom $X/g-C_3N_4$ ($X = Au_1, Pd_1,$ and Ru_1) catalysts are able to improve the catalytic activity of the reaction, which is particularly true for $Au_1/g-C_3N_4$, which was determined as the optimal catalyst. This is consistent with previous reports that an Au-based catalyst may be the ideal candidate for the production of polyvinyl chloride.

Table 2. Comparison of rate-limiting step energy barriers for acetylene hydrochlorination reaction over different catalysts (energies in kcal/mol).

Catalyst	Energy Barrier	Reference
$Au_1/g-C_3N_4$	13.66	This work
$Pd_1/g-C_3N_4$	30.89	This work
$Ru_1/g-C_3N_4$	30.37	This work
$g-C_3N_4/AC$	77.94	[36]
AuG-SAC	30.59	[8]
PSAC-N	28.83	[48]
$AuCl_3$	11.86	[19]

4. Conclusions

In the present study, we investigated the reaction mechanism of the single-atom $X/g-C_3N_4$ ($X = Au_1, Pd_1, \text{ and } Ru_1$) catalysts in an acetylene hydrochlorination reaction. Our calculations and analyses indicate that the mechanism of the three catalysts is similar, in that the C_2H_2 adsorption occurs prior to the adsorption of HCl. This results in co-adsorption and the products are obtained through one intermediate (Ims1) and two transition states (TS1 and TS2). The rate-limiting step of the $Au_1/g-C_3N_4$ and $Pd_1/g-C_3N_4$ catalyzed process is the dissociation of the C_2H_3Cl molecule in the catalyst. On the contrary, the transition from Ims1 to TS2 is the rate-limiting step in the reactions catalyzed by $Ru_1/g-C_3N_4$. Moreover, our results show that the three SACs can enhance the activity of the reaction to varying degrees and the calculated energy barrier decreases in the order of $Pd_1/g-C_3N_4 > Ru_1/g-C_3N_4 > Au_1/g-C_3N_4$. The energy barrier for the reaction catalyzed by the single-atom $Au_1/g-C_3N_4$ catalyst is only 13.66 kcal/mol. In conclusion, in comparison to the other investigated SACs for acetylene hydrochlorination, $Au_1/g-C_3N_4$ exhibited the best performance. We hope that our study provides theoretical support for researching and developing novel SACs.

Author Contributions: M.Z. and L.K. designed and administered the calculations. X.Z. performed the calculations. X.Z. and L.K. collected and analyzed data. All authors discussed the data and wrote the manuscript.

Funding: This research was funded by the National Natural Science Funds of China (NSFC, 21666033), the International Corporation of S&T Project in Xinjiang Bingtuan (grant number 2018BC003), and the International Corporation of S&T Project in Shihezi University (grant number GJHZ201701).

Acknowledgments: This work was supported by the National Natural Science Funds of China (NSFC, 21666033), the International Corporation of S&T Project in Xinjiang Bingtuan (grant number 2018BC003), and the International Corporation of S&T Project in Shihezi University (grant number GJHZ201701).

Conflicts of Interest: The authors declare no conflict of interest.

References

1. Liang, S.; Shi, Y.; Hao, C. The Power of Single-Atom Catalysis. *ChemCatChem* **2015**, *7*, 2559–2567. [[CrossRef](#)]
2. Wang, A.; Li, J.; Zhang, T. Heterogeneous single-atom catalysis. *Nat. Rev. Chem.* **2018**, *2*, 65–81. [[CrossRef](#)]
3. Yang, X.-F.; Wang, A.; Qiao, B.; Li, J.; Liu, J.; Zhang, T. Single-Atom Catalysts: A New Frontier in Heterogeneous Catalysis. *Accounts Chem. Res.* **2013**, *46*, 1740–1748. [[CrossRef](#)] [[PubMed](#)]
4. Huang, Z.; Gu, X.; Cao, Q.; Hu, P.; Hao, J.; Li, J.; Tang, X. Catalytically Active Single-Atom Sites Fabricated from Silver Particles. *Angew. Chem. Int. Ed.* **2012**, *51*, 4198–4203. [[CrossRef](#)]
5. Qiao, B.; Wang, A.; Yang, X.; Allard, L.F.; Jiang, Z.; Cui, Y.; Liu, J.; Li, J.; Zhang, T. Single-atom catalysis of CO oxidation using Pt1/FeOx. *Nat. Chem.* **2011**, *3*, 634–641. [[CrossRef](#)] [[PubMed](#)]
6. Yang, M.; Allard, L.F.; Flytzani-Stephanopoulos, M. Atomically Dispersed Au-(OH)_x Species Bound on Titania Catalyze the Low-Temperature Water-Gas Shift Reaction. *J. Am. Chem. Soc.* **2013**, *135*, 3768–3771. [[CrossRef](#)]
7. Gao, G.; Jiao, Y.; Waclawik, E.R.; Du, A. Single Atom (Pd/Pt) Supported on Graphitic Carbon Nitride as an Efficient Photocatalyst for Visible-Light Reduction of Carbon Dioxide. *J. Am. Chem. Soc.* **2016**, *138*, 6292–6297. [[CrossRef](#)]
8. Gong, W.; Zhao, F.; Kang, L. Novel nitrogen-doped Au-embedded graphene single-atom catalysts for acetylene hydrochlorination: A density functional theory study. *Comput. Theor. Chem.* **2018**, *1130*, 83–89. [[CrossRef](#)]
9. Johnston, P.; Carthey, N.; Hutchings, G.J. Discovery, Development, and Commercialization of Gold Catalysts for Acetylene Hydrochlorination. *J. Am. Chem. Soc.* **2015**, *137*, 14548–14557. [[CrossRef](#)]
10. Malta, G.; Kondrat, S.A.; Freakey, S.J.; Davies, C.J.; Lu, L.; Dawson, S.; Thetford, A.; Gibson, E.K.; Morgan, D.J.; Jones, W.; et al. Identification of single-site gold catalysis in acetylene hydrochlorination. *Science* **2017**, *355*, 1399–1403. [[CrossRef](#)]
11. Conte, M.; Carley, A.; Heirene, C.; Willock, D.; Johnston, P.; Herzing, A.; Kiely, C.; Hutchings, G. Hydrochlorination of acetylene using a supported gold catalyst: A study of the reaction mechanism. *J. Catal.* **2007**, *250*, 231–239. [[CrossRef](#)]

12. Zhao, J.; Xu, J.; Xu, J.; Zhang, T.; Di, X.; Ni, J.; Li, X. Enhancement of Au/AC acetylene hydrochlorination catalyst activity and stability via nitrogen-modified activated carbon support. *Chem. Eng. J.* **2015**, *262*, 1152–1160. [[CrossRef](#)]
13. Malta, G.; Freakley, S.J.; Kondrat, S.A.; Hutchings, G.J. Acetylene hydrochlorination using Au/carbon: A journey towards single site catalysis. *Chem. Commun.* **2017**, *53*, 11733–11746. [[CrossRef](#)] [[PubMed](#)]
14. Wei, X.; Shi, H.; Qian, W.; Luo, G.; Jin, Y.; Wei, F. Gas-Phase Catalytic Hydrochlorination of Acetylene in a Two-Stage Fluidized-Bed Reactor. *Ind. Eng. Chem. Res.* **2009**, *48*, 128–133. [[CrossRef](#)]
15. Zhou, K.; Wang, W.; Zhao, Z.; Luo, G.; Miller, J.T.; Wong, M.S.; Wei, F. Synergistic Gold–Bismuth Catalysis for Non-Mercury Hydrochlorination of Acetylene to Vinyl Chloride Monomer. *ACS Catal.* **2014**, *4*, 3112–3116. [[CrossRef](#)]
16. Zhao, W.; Zhu, M.; Dai, B. Cobalt-nitrogen-activated carbon as catalyst in acetylene hydrochlorination. *Catal. Commun.* **2017**, *98*, 22–25. [[CrossRef](#)]
17. Hutchings, G. Vapor phase hydrochlorination of acetylene: Correlation of catalytic activity of supported metal chloride catalysts. *J. Catal.* **1985**, *96*, 292–295. [[CrossRef](#)]
18. Nkosi, B.; Coville, N.J.; Hutchings, G.J. Reactivation of a supported gold catalyst for acetylene hydrochlorination. *J. Chem. Soc. Chem. Commun.* **1988**, *1*, 71–72. [[CrossRef](#)]
19. Zhang, S.; Zhu, M.; Kang, L.; Su, Y.; Dai, B. MCl_x (M = Hg, Au, Ru; x = 2, 3) catalyzed hydrochlorination of acetylene—A density functional theory study. *Can. J. Chem.* **2013**, *91*, 120–125.
20. Zhu, M.; Wang, Q.; Chen, K.; Wang, Y.; Huang, C.; Dai, H.; Yu, F.; Kang, L.; Dai, B. Development of a Heterogeneous Non-Mercury Catalyst for Acetylene Hydrochlorination. *ACS Catal.* **2015**, *5*, 5306–5316. [[CrossRef](#)]
21. Zhang, J.; Sheng, W.; Guo, C.; Li, W. Acetylene hydrochlorination over bimetallic Ru-based catalysts. *RSC Adv.* **2013**, *3*, 21062. [[CrossRef](#)]
22. Pu, Y.; Zhang, J.; Yu, L.; Jin, Y.; Li, W. Active ruthenium species in acetylene hydrochlorination. *Appl. Catal. A Gen.* **2014**, *488*, 28–36. [[CrossRef](#)]
23. Li, G.; Pu, Y.; Sun, M.; Zhang, H. Non-mercury catalytic acetylene hydrochlorination over Ru catalysts enhanced by carbon nanotubes. *RSC Adv.* **2015**, *5*, 9002–9008. [[CrossRef](#)]
24. Li, G.; Pu, Y.; Jin, Y.; Zhang, J. Effects of potassium additive on the activity of Ru catalyst for acetylene hydrochlorination. *RSC Adv.* **2015**, *5*, 37774–37779.
25. Sun, M.; Han, Y.; Li, W.; Zhang, J. Influence of chlorine coordination number on the catalytic mechanism of ruthenium chloride catalysts in the acetylene hydrochlorination reaction: A DFT study. *Phys. Chem. Chem. Phys.* **2015**, *17*, 7720–7730.
26. Xu, J.; Zhang, T.; Di, X.; Gu, S.; Zhao, J.; Ni, J.; Li, X. Ultra-low Ru-promoted CuCl₂ as highly active catalyst for the hydrochlorination of acetylene. *RSC Adv.* **2015**, *5*, 38159–38163. [[CrossRef](#)]
27. Wang, L.; Wang, F.; Wang, J.; Tang, X.; Zhao, Y.; Yang, D.; Jia, F.; Hao, T. Hydrochlorination of acetylene to vinyl chloride over Pd supported on zeolite Y. *React. Kinet. Mech. Catal.* **2013**, *110*, 187–194. [[CrossRef](#)]
28. Wang, L.; Wang, F.; Wang, J. Catalytic properties of Pd/HY catalysts modified with NH₄F for acetylene hydrochlorination. *Catal. Commun.* **2015**, *65*, 41–45. [[CrossRef](#)]
29. Hu, J.; Yang, Q.; Yang, L.; Zhang, Z.; Su, B.; Bao, Z.; Ren, Q.; Xing, H.; Dai, S. Confining Noble Metal (Pd, Au, Pt) Nanoparticles in Surfactant Ionic Liquids: Active Non-Mercury Catalysts for Hydrochlorination of Acetylene. *ACS Catal.* **2015**, *5*, 6724–6731. [[CrossRef](#)]
30. Wang, Y.; Zhu, M.; Kang, L.; Dai, B. Neutral Aun (n = 3–10) clusters catalyze acetylene hydrochlorination: A density functional theory study. *RSC Adv.* **2014**, *4*, 38466–38473. [[CrossRef](#)]
31. Zhao, Y.; Zhao, F.; Kang, L. Catalysis of the acetylene hydrochlorination reaction by Si-doped Au clusters: A DFT study. *J. Mol. Model.* **2018**, *24*, 61. [[CrossRef](#)] [[PubMed](#)]
32. Fei, Z.; Yang, W.; Lihua, K. A density functional theory study on the performance of graphene and N-doped graphene supported Au₃ cluster catalyst for acetylene hydrochlorination. *Can. J. Chem.* **2016**, *94*, 842–847.
33. Ma, X.; Lv, Y.; Xu, J.; Liu, Y.; Zhang, R.; Zhu, Y. A Strategy of Enhancing the Photoactivity of g-C₃N₄ via Doping of Nonmetal Elements: A First-Principles Study. *J. Phys. Chem. C* **2012**, *116*, 23485–23493. [[CrossRef](#)]
34. Wang, X.; Blechert, S.; Antonietti, M. Polymeric Graphitic Carbon Nitride for Heterogeneous Photocatalysis. *ACS Catal.* **2012**, *2*, 1596–1606. [[CrossRef](#)]

35. Zheng, Y.; Jiao, Y.; Chen, J.; Liu, J.; Liang, J.; Du, A.; Zhang, W.; Zhu, Z.; Smith, S.C.; Jaroniec, M.; et al. Nanoporous Graphitic-C₃N₄@Carbon Metal-Free Electrocatalysts for Highly Efficient Oxygen Reduction. *J. Am. Chem. Soc.* **2011**, *133*, 20116–20119. [[CrossRef](#)] [[PubMed](#)]
36. Li, X.; Wang, Y.; Kang, L.; Zhu, M.; Dai, B. A novel, non-metallic graphitic carbon nitride catalyst for acetylene hydrochlorination. *J. Catal.* **2014**, *311*, 288–294. [[CrossRef](#)]
37. Zhao, W.; Zhu, M.; Dai, B. The Preparation of Cu-g-C₃N₄/AC Catalyst for Acetylene Hydrochlorination. *Catal.* **2016**, *6*, 193. [[CrossRef](#)]
38. Zheng, Y.; Jiao, Y.; Zhu, Y.; Cai, Q.; Vasileff, A.; Li, L.H.; Han, Y.; Chen, Y.; Qiao, S.-Z. Molecule-Level g-C₃N₄ Coordinated Transition Metals as a New Class of Electrocatalysts for Oxygen Electrode Reactions. *J. Am. Chem. Soc.* **2017**, *139*, 3336–3339. [[CrossRef](#)] [[PubMed](#)]
39. Li, S.-L.; Yin, H.; Kan, X.; Gan, L.-Y.; Schwingenschlög, U.; Zhao, Y. Potential of transition metal atoms embedded in buckled monolayer g-C₃N₄ as single-atom catalysts. *Phys. Chem. Chem. Phys.* **2017**, *19*, 30069–30077. [[CrossRef](#)]
40. Frisch, M.J.; Trucks, G.W.; Schlegel, H.B.; Scuseria, G.E.; Robb, M.A.; Cheeseman, J.R.; Scalmani, G.; Barone, V.; Mennucci, B.; Petersson, G.A.; et al. *Gaussian 09. Revision C.01*, Gaussian Inc.: Wallingford, CT, USA, 2010.
41. Lee, C.; Yang, W.; Parr, R.G. Development of the Colle-Salvetti correlation-energy formula into a functional of the electron density. *Phys. Rev. B* **1988**, *37*, 785–789. [[CrossRef](#)] [[PubMed](#)]
42. Antony, J.; Krieger, H.; Grimme, S.; Ehrlich, S. A consistent and accurate ab initio parametrization of density functional dispersion correction (DFT-D) for the 94 elements H-Pu. *J. Chem. Phys.* **2010**, *132*, 154104.
43. González, C.; Schlegel, H.B. An improved algorithm for reaction path following. *J. Chem. Phys.* **1989**, *90*, 2154–2161. [[CrossRef](#)]
44. Gonzalez, C.; Schlegel, H.B. Reaction path following in mass-weighted internal coordinates. *J. Phys. Chem.* **1990**, *94*, 5523–5527. [[CrossRef](#)]
45. Kroke, E.; Schwarz, M.; Horath-Bordon, E.; Kroll, P.; Noll, B.; Norman, A.D. Tri-s-triazine derivatives. Part I. From trichloro-tri-s-triazine to graphitic C₃N₄ structures. *New J. Chem.* **2002**, *26*, 508–512. [[CrossRef](#)]
46. Zhao, Y.; Zhu, M.; Kang, L. The DFT Study of Single-Atom Pd₁/g-C₃N₄ Catalyst for Selective Acetylene Hydrogenation Reaction. *Catal. Lett.* **2018**, *148*, 2992–3002. [[CrossRef](#)]
47. Gracia, J.; Kroll, P. Corrugated layered heptazine-based carbon nitride: The lowest energy modifications of C₃N₄ ground state. *J. Mater. Chem.* **2009**, *19*, 3013. [[CrossRef](#)]
48. Wang, X.; Dai, B.; Wang, Y.; Yu, F. Nitrogen-Doped Pitch-Based Spherical Active Carbon as a Nonmetal Catalyst for Acetylene Hydrochlorination. *ChemCatChem* **2014**, *6*, 2339–2344. [[CrossRef](#)]



© 2019 by the authors. Licensee MDPI, Basel, Switzerland. This article is an open access article distributed under the terms and conditions of the Creative Commons Attribution (CC BY) license (<http://creativecommons.org/licenses/by/4.0/>).